Int. J. Heat Mass Transfer. Vol. 15, pp. 2251–2269. Pergamon Press 1972. Printed in Great Britain

NUMERICAL SIMULATION OF DROPWISE CONDENSATION

LEON R. GLICKSMAN and ANDREW W. HUNT, JR.*

Department of Mechanical Engineering, Massachusetts Institute of Technology, Cambridge, Massachusetts 02139, U.S.A.

(*Received* 26 *November* 1971)

Abstract—A numerical simulation of dropwise condensation heat transfer was performed. The simulation accounts for growth, coalescence, and renucleation of drops ranging in size from the smallest nucleating drops to departing drops. The calculations were performed with an active site density as high as 10^9 sites/cm^2.

Heat transfer to the drop was determined by considering the effects of curvature of the drop surface, interfacial mass transfer between the liquid and vapor phases, and conduction through the drop. The effects of non-condensibles in the vapor and non-uniform conduction in the condensing surface material were omitted.

The heat transfer coefficient was found as a function of the active site density, the saturation temperature, the departing drop size, and the vapor to surface temperature difference. The results agree well with available experimental results.

NOMENCLATURE

A, cross sectional area [μ^2];
D_{max}, maximum or departing drop diameter [μ];
h, instantaneous heat transfer coefficient [Btu/hft^2°F];
$\bar{h}$, time averaged heat transfer coefficient [Btu/hft^2°F];
h_{fg}, heat of vaporization [Btu/lb$_m$];
K, thermal conductivity [Btu/hft°F];
M, molecular weight;
N_D, number of drops;
N_L, number of locations;
Q, heat transfer rate [Btu/h];
r, drop radius [μ];
r_{min}, minimum drop radius [μ];
$\bar{R}$, universal gas constant [Btu/lb$_m$°F];
S, conduction shape factor;
T, temperature [°F];
T_s, saturation temperature [°R];
t, time [s];
v_g, specific volume of vapor [ft^3/lb$_m$].

Greek letters

α, condensation coefficient;
α, inclination angle [degrees];
θ, contact angle [degrees];
ρ, density [lb$_m$/ft^3];
σ, surface tension [lb$_f$/ft];
τ, time period [s].

Subscripts

A, advancing;
C, curvature;
CD, conduction;
i, interfacial;
R, receding;
t, total.

1. INTRODUCTION

DROPWISE condensation has attracted considerable interest since it was established that the heat transfer coefficient for dropwise condensation is an order of magnitude larger than that for filmwise condensation [1].

Experimental investigations of dropwise condensation have revealed that the heat transfer

* Presently Lt., U.S. Navy.

coefficient is a function of vapor pressure [2, 3], vapor-to-surface temperature difference [2, 4–7], surface inclination [8, 9], and non-condensible gases [2, 6] among others. It has also been demonstrated that vapor condenses at discrete nucleation sites on a bare surface and that films thicker than a monolayer cannot exist in the area between drops [10–13].

The primary drops which condense at nucleation sites have diameters of one micron or less. Observing the surface with a microscope, one can see small drops grow and coalesce with their neighbors. New small drops appear in the area uncovered by coalescences. The large drops continue to grow and coalesce with each other and with the new small drops. When the largest drop reaches a size at which the gravity force exceeds the surface tension forces holding the drops to the surface, the drop slides down the surface sweeping other drops with it. The swept area is bare and the cycle begins anew. The ratio of the departing drop diameter to the primary drop diameter is greater than one thousand to one.

To obtain a thorough understanding of the mechanism of dropwise condensation, it is necessary to be able to predict the heat transfer coefficient from first principles. Considerable progress has been made to calculate the heat transfer through a single drop of a given size. Effects of liquid conduction, curvature of the interface, interfacial mass transfer resistance, and non-uniform conduction in the condensing surface can be accounted for. However, to calculate the average heat transfer for the entire surface, the distribution of drops by sizes from the smallest primary drops to the largest departing drops must also be known.

Early attempts at calculating the heat transfer assumed all the drops on a surface were uniform in size and spacing [14–16]. Le Fevre and Rose [17] assumed a form for the distribution function. Glicksman and Rose [18] found a universal form of the distribution function for large drops which grow primarily by coalescence with smaller drops. The predicted distribution is not valid for small drops which grow by direct condensation.

Gose, Mucciardi, and Baer [19] and Tanasawa and Tachibana [20] have attempted to model the growth and coalescence by computer. Both works modeled drops of the entire range of sizes on a fixed area. The computer facility limited their investigations to artificially low site densities on the order of 10^4 sites per cm^2. A recent estimate of the active nucleation site density is of the order of 10^7–10^8 sites per cm^2 [2]. The calculated heat transfer coefficients of Gose and Tanasawa are at least an order of magnitude lower than experimentally observed values.

This paper presents a numerical simulation of dropwise condensation in which large nucleation site densities and the growth of large drops is accounted for. The simulation model will first be described in general, the calculation of drop nucleation and growth will be discussed, and the details of the simulation will be presented. The results of the calculation will be compared with recent experimental data.

2. THE MODEL

A representative model of a condensing surface one square centimeter in area with 10^8 sites/cm^2 would require approximately one hundred million condensing sites. Clearly, a computer program which would account for the nucleation, growth, coalescence, and renucleation of all of the sites on one square centimeter is out of the question. The calculation would become more reasonable if the site density were reduced or if the area under study were decreased. Previous studies have shown that a reduction of the site density gives very inaccurate results. If an area much smaller than one square centimeter were modeled, the growth of large drops could not be accounted for.

The present simulation models a single cycle of the condensation process from nucleation on an initially bare surface to formation of a drop of the departing size. To solve the formidable computational difficulties, the condensation process is modeled by a series of stages. The

stages correspond to successive time periods of the cycle, each containing larger drops than the preceding stage. In the first stage, the nucleation, growth, coalescence, and renucleation of small primary drops is studied. The first stage contains one thousand randomly distributed nucleation sites; the area of the first stage varies inversely with nucleation site density.

The surface of the first stage is assumed to be initially bare as if it were swept by a falling drop or uncovered by the coalescence of two large drops. Growth, coalescence, and renucleation of primary drops proceeds until drops are formed which are large for this stage. The growth of the large drops from the first stage is continued on the second stage, which has an area ten times larger than the first stage. Nucleation and growth of primary drops cannot be followed in detail because the number of nucleation sites has been increased tenfold. The average behavior of primary drops can be accounted for by using the results of the first stage. The simulation is continued by using stages with successively larger areas. When a drop is formed which is equal to the size of a departing drop as found by experiments, the condensation cycle is complete and the program is terminated. The stages used for condensation on a surface with a site density of 10^8 sites per square centimeter are shown on Table 1. The growth and coalescence of only the largest drops are considered in detail no matter how many nucleation sites are contained in a given stage.

Table 1. Calculation stages for a nucleation site density of 10^8 sites per square centimeter

Stage number	Stage area (μ^2)	Size of drops considered in detail radius (μ)
1	10^3	$0{\cdot}10 \leqslant R \leqslant 3{\cdot}75$
2	10^4	$1{\cdot}59 \leqslant R \leqslant 12{\cdot}04$
3	10^5	$8{\cdot}03 \leqslant R \leqslant 40{\cdot}64$
4	10^6	$27{\cdot}10 \leqslant R \leqslant 137{\cdot}17$
5	10^7	$91{\cdot}45 \leqslant R \leqslant 462{\cdot}96$
6	$3{\cdot}24 \times 10^8$	$308{\cdot}64 \leqslant R \leqslant 1250{\cdot}00$

The analysis is based on the assumption that condensation in the area between the largest drops of a stage can be found from the average condensation rate of the previous stage. The presence of large drops is assumed to have a negligible influence on the heat transfer to small drops in the surrounding area. Large drops do cause an increased resistance to conduction in the condensing surface [21]. However, for surface materials with high thermal conductivity, this effect is minimal.

3. DROP NUCLEATION AND GROWTH

The minimum size and the growth of drops are governed by the heat transfer relations for a single drop. The heat transfer to a drop is determined by the effects of curvature, interfacial mass transfer between the liquid and vapor phases, conduction through the drop, non-condensibles in the vapor, and non-uniform conduction in the material forming the condensing surface. The effects of noncondensibles and non-uniform conduction have been omitted from this study. Curvature of the liquid–vapor interface results in an equilibrium saturation temperature which is lower than the saturation temperature at a planar interface. A drop of water in equilibrium with vapor at one atmosphere is at a temperature lower than 212°F. The difference in the equilibrium temperature of saturated vapor at a planar interface and at a curved interface is given by:

$$\Delta T_c = \frac{2T_s\sigma}{h_{fg}\rho}\frac{1}{r}. \tag{1}$$

Saturation temperature will refer to equilibrium at a planar surface for the balance of this paper.

This is a pressure difference necessary to achieve a net mass transfer from vapor to liquid at the interface. This can be converted into a temperature difference, which is [10]:

$$\Delta T_i = \frac{\sigma}{h_i 2\pi r^2} \tag{2}$$

where h_i is the interfacial heat transfer coefficient which can be calculated from [22]:

$$h_i = \left(\frac{2\alpha}{2-\alpha}\right)\left(\frac{M}{2\pi\bar{R}T_s}\right)^{\frac{1}{2}}\frac{h_{fg}^2}{T_s v_g}. \tag{3}$$

Based on the most recent data [23], α, the condensation coefficient, will be taken as unity. For water, h_i is $2{\cdot}7 \times 10^6$ Btu/(hft^2°F) at 212°F and $2{\cdot}7 \times 10^5$ Btu/(hft^2°F) at 88°F.

The temperature drop due to conduction through the drop can be expressed as:

$$\Delta T_{CD} = \frac{QS}{K\pi r}. \tag{4}$$

The shape factor, S, has been determined to be one-quarter for hemispherical drops [21].

The total temperature drop from vapor at its saturation temperature to the solid condensing surface is the sum of the temperature differences due to curvature, interfacial mass transfer, and conduction [17]:

$$\Delta T_t = \Delta T_c + \Delta T_i + \Delta T_{CD}. \tag{5}$$

The heat transfer rate for a drop can be found from equations (1), (2), (4) and (5) as:

$$Q = \frac{\Delta T - \dfrac{2T_s\sigma}{h_{fg}\rho}\dfrac{1}{r}}{\dfrac{1}{h_i 2\pi r^2} + \dfrac{1}{4K\pi r}}. \tag{6}$$

The heat transfer per unit of surface area occupied by a hemispherical drop is shown on Fig. 1. For large drops, conduction is the dominating resistance to heat transfer. Curvature and interfacial effects cannot be neglected when modeling the growth of primary drops.

A drop has zero growth rate when the total temperature difference equals the temperature difference due to curvature. The minimum size drop which can exist on a surface is one with zero growth rate. From equation (1):

$$r_{\min} = \frac{2T_s\sigma}{h_{fg}\rho(\Delta T_t)}. \tag{7}$$

The rate of growth of a hemispherical drop is given by

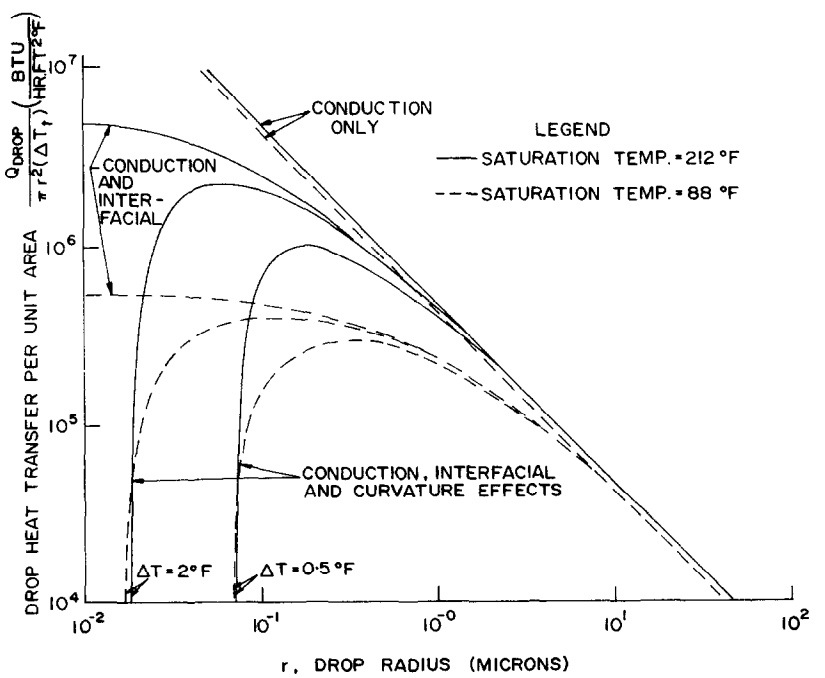

FIG. 1. Drop heat transfer per unit condensing surface area.

$$\rho h_{fg} 2\pi r^2 \frac{dr}{dt} = Q \tag{8}$$

$$\frac{dr}{dt} = \frac{Q}{\pi r^2} \frac{1}{(2\rho h_{fg}} \tag{9}$$

Since drops with a radius exactly equal to r_{min} do not grow, only primary drops with a nucleation radius greater than r_{min} are active. Figure 2 illustrates the growth of two drops,

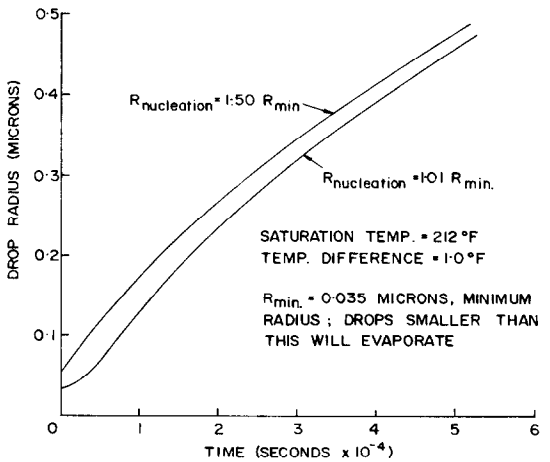

FIG. 2. Effect of nucleation radius on drop growth.

the first with a nucleation radius 1 per cent greater than r_{min} and the second with a nucleation radius 50 per cent greater than r_{min}. Thus, the choice of the nucleation radius is not critical in predicting the growth and heat transfer to an individual drop.

4. THE SIMULATION

The simulation commences with nucleation of primary drops on the first stage. The first stage is a square containing one thousand randomly distributed nucleation sites whose locations are determined from a six-place random number generator. The use of one thousand sites minimizes edge effects and gives a sample size large enough to eliminate significant statistical fluctuations.

The first stage calculation is begun by assuming all primary drops have a nucleation radius fifty per cent larger than the minimum radius. The drops are hemispheres, and they are always centered on the nucleation sites. A small time step is taken, and the drop growth is calculated from the integrated form of equation (9).

Coalescence

A check for coalescences between drops is made after every time step. A square two diameters on a side is centered around a drop, and overlap with equal sized or smaller drops which have centers in the square is checked. Drops which overlap are combined with the center drop to form a new drop at the center. After each coalescence the search area is enlarged. When the central drop fails to coalesce with any drop in the search square, the routine continues to the next drop. When every drop on the surface has been used as a search center, the coalescence check is complete. The program is efficient since small search areas are used for the numerous small drops, while large search areas are used only for the comparatively few large drops.

The time steps for the first stage must be short or the primary drops will overlap by a large amount. Since drops actually coalesce upon first touching, long time steps will lead to errors, particularly for high site densities.

The coalescences uncover nucleation sites upon which primary drops grow during the next time step. Growth, coalescence, and renucleation is continued until either a single drop covers more than 4·55 per cent of the stage area, or seven drops cover twenty per cent of the stage area. Border effects are minimized by terminating the stage before comparatively large drops are formed.

The amount of heat transferred through the condensing surface can be determined from the increase in the mass of the drops. This in turn can be used to calculate the instantaneous and time averaged heat transfer coefficients. The average heat transfer coefficient is defined as:

$$\bar{h}(\tau) = \frac{1}{\tau} \int_0^{\tau} \frac{Q(t)\,dt}{A(\Delta T)_t} = \frac{1}{\tau} h(t)\,dt. \tag{10}$$

Zero time corresponds to the beginning of the first stage.

Figure 3 illustrates the behavior of the time averaged heat transfer coefficient for the first stage. The effect of using different time steps and

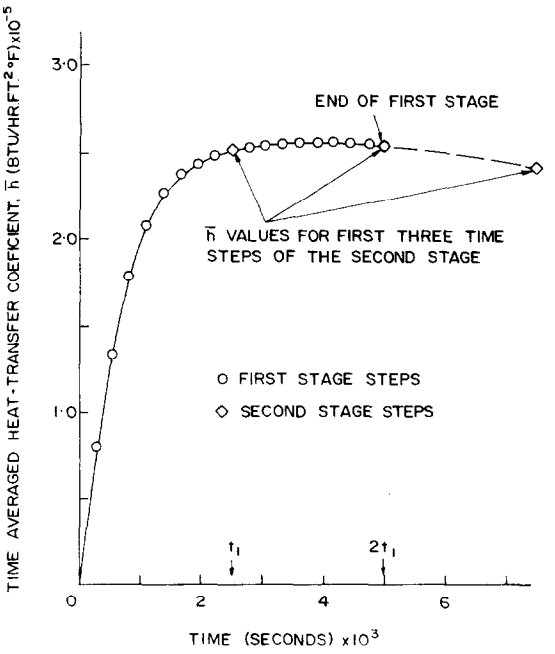

FIG. 3. Growth of first stage and startup of second stage; second stage grows with time steps of t_1.

different areas, with the same site density, is shown on Fig. 4. In subsequent cases, a time step of either 0·05 or 0·1 ms was made for the first stage, and the first stage area contained one thousand active nucleation sites.

The second stage

Since the area of the second stage is ten times the first stage, nucleation cannot be studied in detail. The growth and coalescence of the largest drops are followed in detail, and in the area unoccupied by the largest drops the average heat flux per unit area is taken from the result of the first stage.

The starting conditions of the second stage are determined by an iterative procedure which matches the average heat transfer of the first and second stage at two different times. The second stage starts at time t_1, which is one-half the total time for the first stage (see Fig. 3). The drops on the second stage at time t_1 are assumed to be uniform in size with a radius r_2. The number of drops, N_2, is calculated so that the total amount of liquid on the surface at time t_1 is the same for the first and second stage; thus the average heat transfer coefficient of the first and second stage is equal at t_1.

All of the drops are distributed on a uniformly spaced net of locations to ensure that none of the drops coalesce immediately after being placed on the surface. The number of locations, N_L, is larger than the number of drops, N_D, so random numbers are used to determine if a drop is present at a particular location.

A time step of duration t_1 is taken and drops grow by condensation. The heat transfer to the area unoccupied by the N_D drops is calculated by using the average heat flux per unit area for the first stage at time t_1. The heat transfer to the unoccupied area results in condensation which is accounted for by placing drops of radius r_2 on unoccupied locations. The average heat transfer coefficient at time $2t_1$ is calculated for the second stage and compared to the value found for the first stage. If the values disagree, a new radius r_2 is assumed and the second stage start-up is repeated until the average heat transfer coefficient at times t_1 and $2t_1$ is the same for the first and second stages.

The time is increased by steps equal to t_1 and the evolution of the second stage proceeds with growth and coalescence of existing drops and creation of new drops on the area unoccupied by existing drops. All new drops are added to the surface at the radius r_2. The termination for the second stage is identical to the criteria for the first stage. The third stage has an area ten times the area of the second stage, and the time steps are equal to one-half the total time of the second stage. The startup of the third stage is exactly the same as the second stage, with the average condensation rate on the unoccupied area found from the results of the second stage.

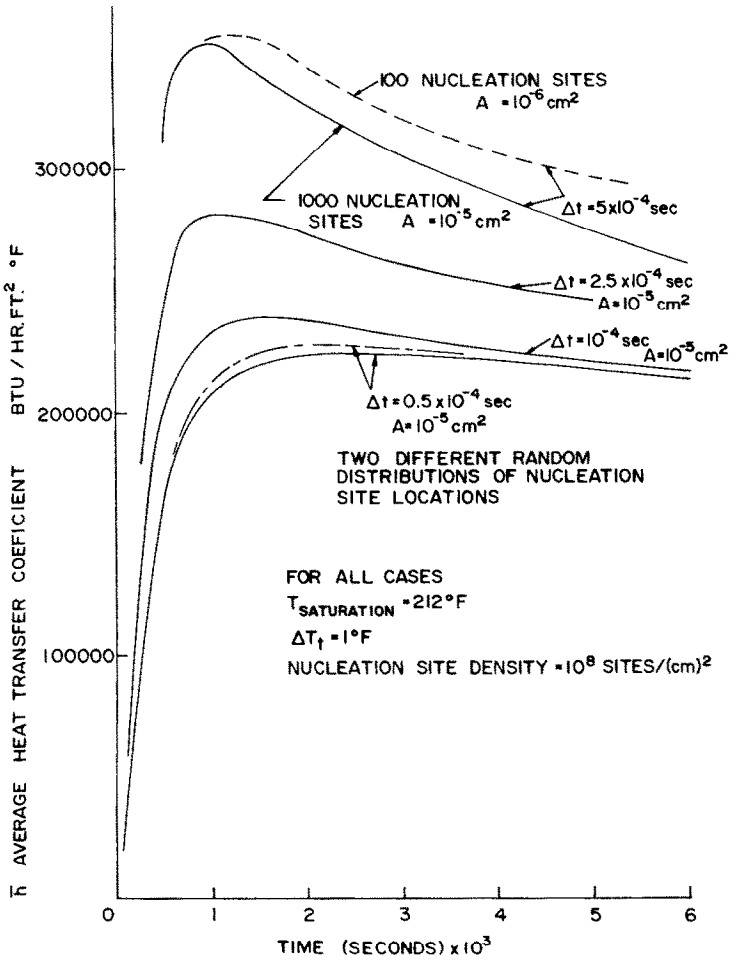

FIG. 4. Growth of first stage, effects of simulation time steps, stage area, and distribution of sites.

Succeeding stages are similar to the third stage: each has a larger area and uses a larger time step. The final stage area is three and one-quarter square centimeters, which approximates the size of the surface area used in recent experiments [2, 9]. The last stage terminates when a drop of the departing size is first formed; the size of the departing drops is based on experimental measurements [2].

5. RESULTS

A. *The first stage*

The behaviour of the first stage is shown on Fig. 5 for a typical set of operating conditions. The fluctuations are due to coalescences between relatively large drops during a time step. Initially the surface is covered by small drops which have a large heat transfer rate per unit of occupied surface area (Fig. 1). However, the heat transfer coefficient for the entire condensing surface is limited by the small percentage of area occupied by the drops. As the drops increase in size, the heat transfer increases because the heat transfer per drop increases monotonically with drop size (Fig. 6) and the number of drops is relatively constant.

The percent of surface area covered by drops approaches a constant value and the number of

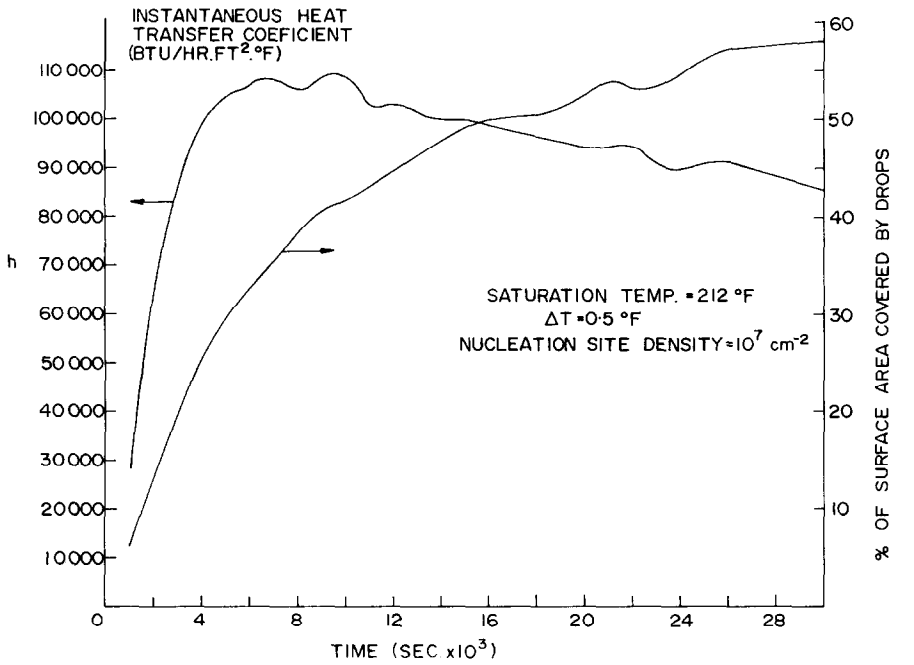

FIG. 5. Instantaneous heat transfer coefficient and per cent of area covered by drops for the first stage.

large drops decreases as drops coalesce with each other more frequently. The heat transfer rate, now limited by the heat transfer rate per unit of occupied surface area, decreases as the average drop size increases.

Surfaces with large nucleation site densities have a much larger percentage of the surface area occupied by small drops producing higher heat transfer rates.

B. *The complete cycle*

The instantaneous heat transfer coefficient and the time averaged heat transfer coefficient were found for a complete cycle from nucleation on a bare surface to production of a drop of departing size. The instantaneous heat transfer coefficient is initially low. It rapidly increases during the first stage, and steadily decreases during the later stages. The steady decrease is caused by the presence of large drops which have a very low heat transfer rate per unit of occupied area. The large drops reduce the area available to small active drops causing a decrease in the overall heat transfer rate to the condensing surface. The large drops continue to grow by coalescing with smaller active drops which grow until they touch the large drops. Eventually, large drops touch each other and coalesce to form even larger drops.

The variation of the average heat transfer coefficient during one complete cycle is shown on Fig. 7 for four assumed active nucleation site densities at a saturation temperature of 212°F. Each curve is terminated when a drop of the departing size appears on the surface. The time for a complete cycle is shorter at high site densities because the average condensation rate increases with increased site densities.

Similar results are shown on Fig. 8 for a saturation temperature of 88°F. The interfacial heat transfer coefficient decreases as the saturation temperature decreases, causing a reduction in the heat transfer to small active drops.

C. *Site density*

The heat transfer coefficient averaged over an entire cycle varies considerably with active site density, as shown in Fig. 9. The predicted average heat transfer coefficient at one atmosphere varies approximately as the site density to the one-third power in the range from 10^5 to 10^9 sites per cm^2. The slope of the predicted curve agrees closely with the data of Krischer and Grigull [24]. Since the data was taken at very low overall temperature differences, a significant uncertainty in the measured temperature difference and in the magnitude of the calculated heat transfer coefficient is to be expected. It will be shown later that for a fixed value of the active site density, the predicted heat transfer coefficient is insensitive to changes in the overall temperature difference.

Photographs taken by Graham [2] were measured by the senior author. Results for a saturation temperature of 88°F and 212°F are shown; the disagreement between the data and the predicted values at higher heat transfer coefficients will be explained in a later section.

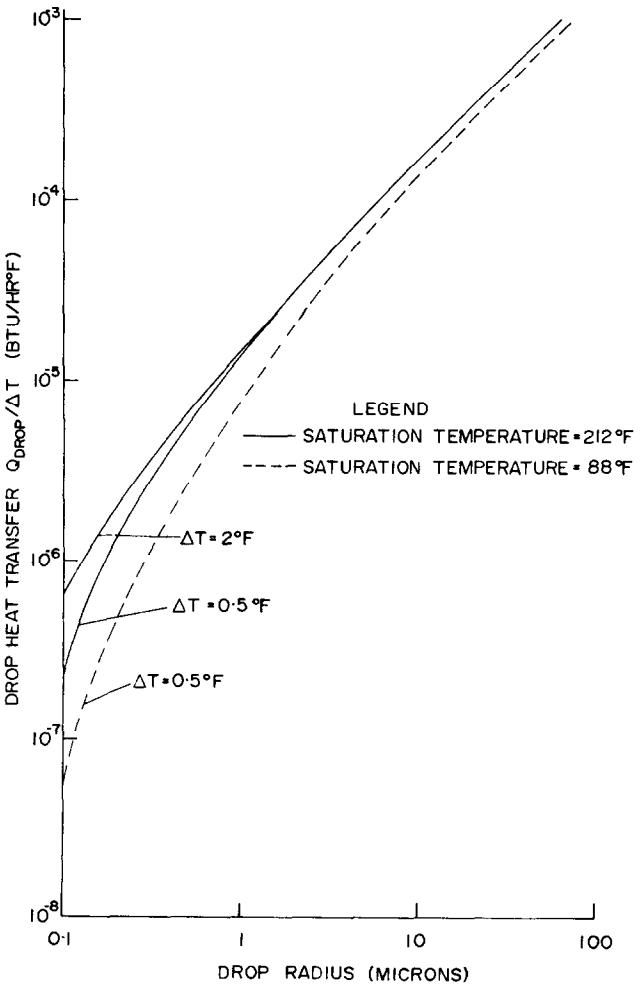

FIG. 6. Heat transfer rate to a single drop.

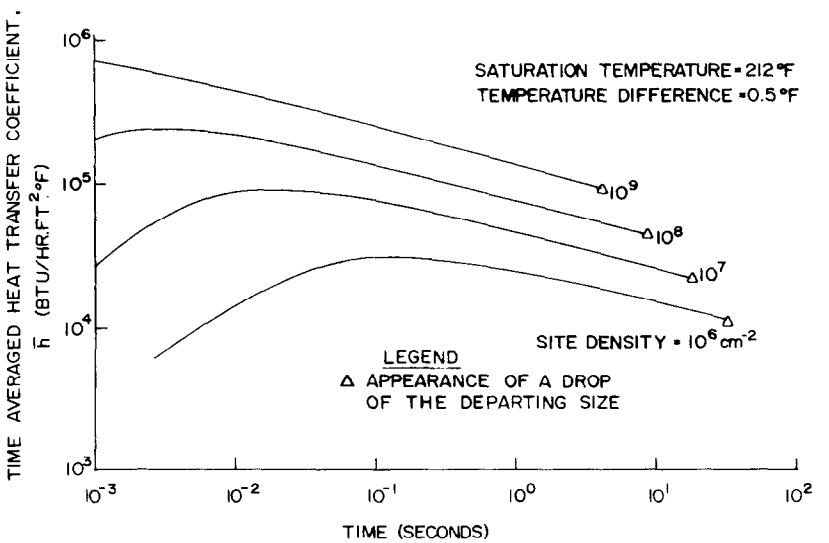

FIG. 7. Time averaged heat transfer coefficient for a complete cycle with a saturated temperature of 212°F.

The maximum theoretical values presented on Fig. 9 were calculated for equal sized drops just touching each other in an equilateral triangular array on the surface. The maximum heat transfer occurs when the number of drops is high and the drop radius is small; for the theoretical maximum the number of drops was assumed to be equal to the number of nucleation sites. The theoretical maximum is the upper limit of the instantaneous heat transfer coefficient; the maximum time averaged heat transfer coefficient would be smaller.

The active site density is an important variable which must be included in any correlation of

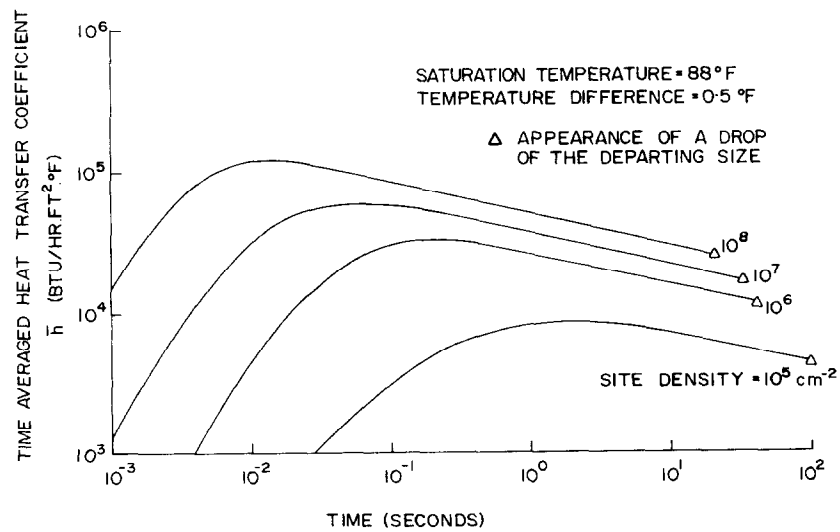

FIG. 8. Time averaged heat transfer coefficient for a complete cycle with a saturation temperature of 88°F.

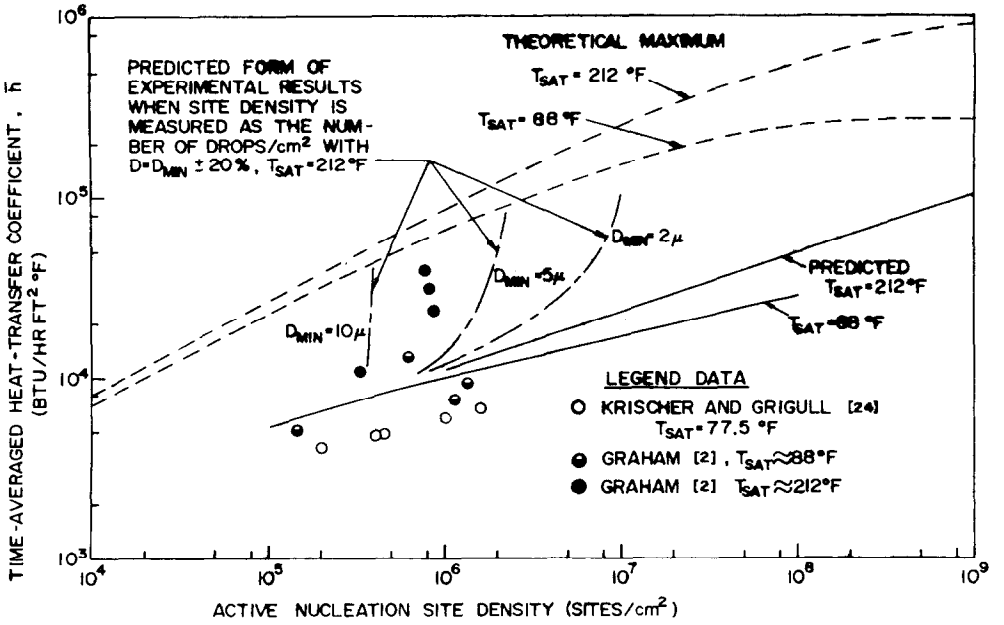

FIG. 9. Predicted and experimental dependence of the time averaged heat transfer coefficient on the active nucleation site density. For all predicted values $\Delta T_i = 0{\cdot}5$°F and $D_{max} = 2500\ \mu$.

experimental results. Differences heretofore attributed to the presence of non-condensible gases may be in fact caused by differences in the active nucleation site density. Of course, very low heat transfer coefficients measured by early investigators must be attributed to the presence of non-condensibles.

D. *Experimental determination of nucleation site density*

The active nucleation site density is experimentally determined by counting the number of just visible drops on a photograph taken at high magnification. The nucleation site density is then assumed to be approximately equal to the drop density in an area heavily populated by these small drops. The results of the present model indicate that this technique is not valid for large active site densities. Table 2 presents the highest instantaneous drop densities found in the calculations for various nucleation site densities. At high nucleation site densities, many coalescences occur before drops of one micron are produced, causing the drop density to be significantly less than the active site density. Clearly, if the nucleation site density is to be measured, some means must be found to identify and count drops less than one micron in radius.

The predicted form for the experimental results of $\bar{h}$ v. measured site density can be derived using Table 2. As the actual site density increases,

Table 2. Maximum predicted drop density
$\Delta T = 0{\cdot}5\ F, T_{saturation} = 212°F, r_{nuc} = 1{\cdot}5 r_{min.}$

Nucleation site density (cm^{-2})	Maximum number of drops (@$R \pm 20\%$)/cm^2 drop radius (μ)		
	1	2·5	5·0
10^6	$8{\cdot}1 \times 10^5$	$7{\cdot}4 \times 10^5$	$3{\cdot}6 \times 10^5$
10^7	$3{\cdot}6 \times 10^6$	$1{\cdot}4 \times 10^6$	$3{\cdot}3 \times 10^5$
10^8	$7{\cdot}6 \times 10^6$	$2{\cdot}3 \times 10^6$	$2{\cdot}2 \times 10^5$
10^9	$1{\cdot}0 \times 10^7$	$2{\cdot}0 \times 10^6$	$3{\cdot}7 \times 10^5$
Maximum drop density: drops in a close packed hexagonal array	$2{\cdot}9 \times 10^7$	$4{\cdot}65 \times 10^6$	$1{\cdot}16 \times 10^6$

the measured site density approaches an upper limit determined by the minimum size of the drops which are counted. The expected behavior of experimental data is shown on Fig. 9. The data of Graham at high heat transfer coefficient has clearly reached an upper limit on the measured site density.

The comments of this section are valid only when the radius of the primary nucleating drops is well below the radius which can be observed. This condition prevails if the nucleation radius is the same order of magnitude as the minimum radius predicted by equation (7); when the temperature difference is greater than one-half degree Fahrenheit, r_{min} is less than one-tenth of a micron.

E. *Distribution of drop sizes*

The time averaged distribution of drop sizes over the complete cycle is shown on Figs. 10 and 11 for saturation temperatures of 212°F and 88°F, respectively. Notice that a universal distribution of drop sizes appears to hold for drops with radii greater than twenty microns. The

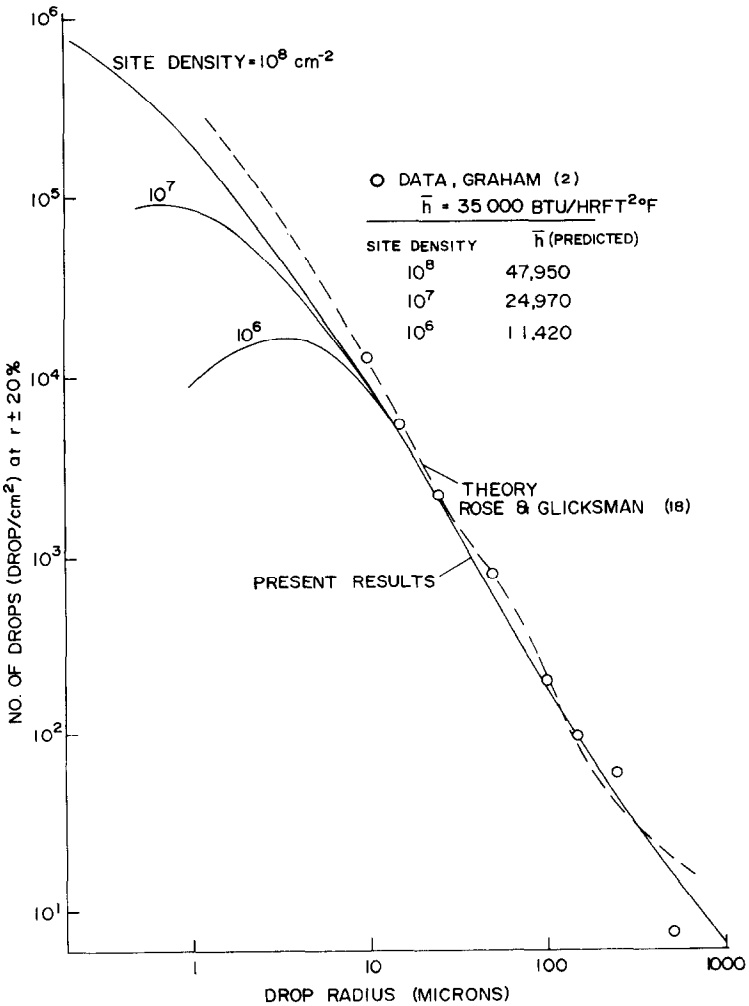

FIG. 10. Average distribution of drop sizes at a saturation temperature of 212°F.

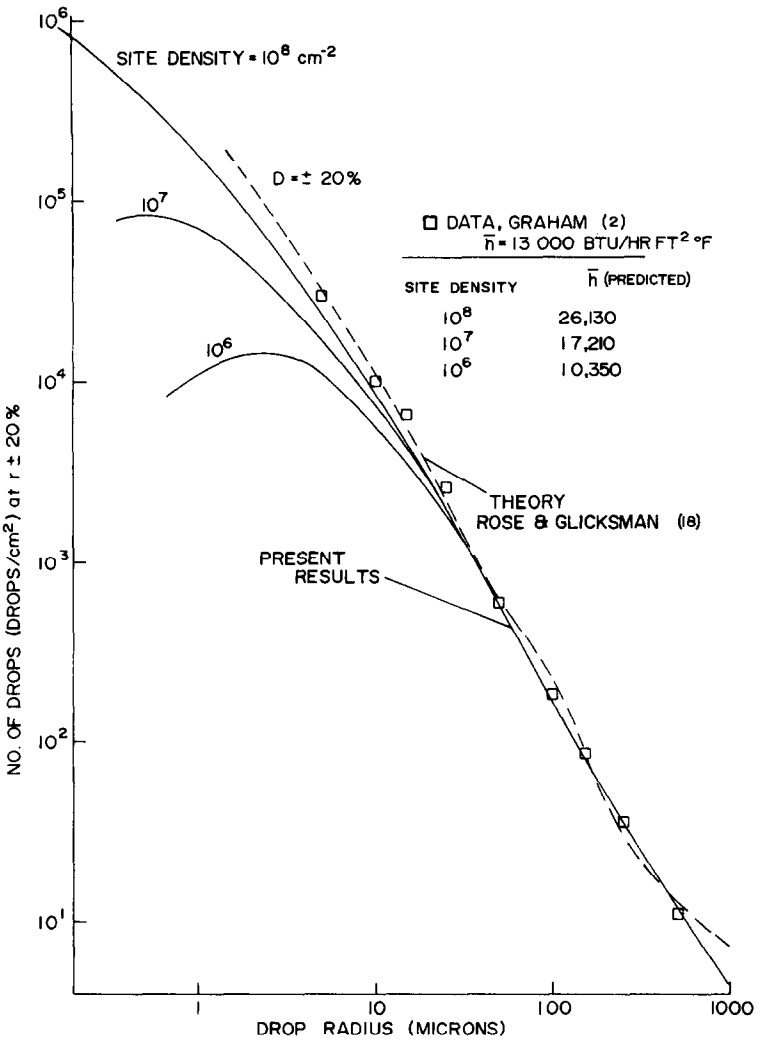

FIG. 11. Average distribution of drop sizes at a saturation temperature of 88°F.

divergence of the distributions at low radii accounts for the differences in the average heat transfer coefficient. The agreement of the predicted distributions and the data of Graham [2] which is averaged over a number of cycles indicates that the prediction for a single cycle is identical to the results for the steady state process. Also shown on the figures is the universal distribution predicted by Glicksman and Rose [18]. The latter prediction is valid for large drops which grow only by coalescence, not by direct condensation.

F. *Saturation temperature*

The influence of saturation temperature on the heat transfer coefficient is shown on Fig. 12.

The predicted values at a constant active site density show a modest decrease with saturation temperature due to changes in the interfacial heat transfer coefficient. However, the experimental results show a more marked decrease in heat transfer coefficient, indicating that the active nucleation site density decreases with decreasing saturation temperature.

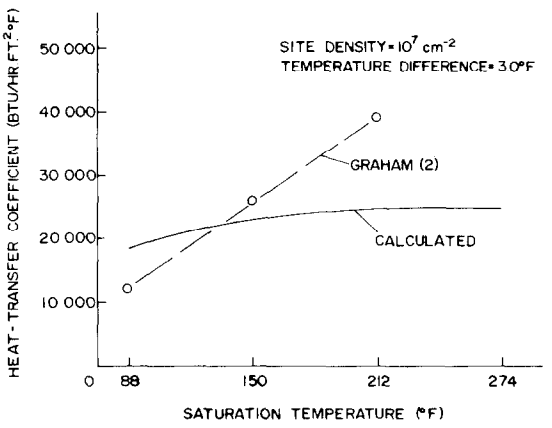

FIG. 12. Variation of time-averaged heat transfer coefficient with saturation temperature.

G. *Temperature difference*

Heat transfer coefficients were calculated for several values of the total temperature differences between the vapor and the surface at saturation temperatures of 88°F and 212°F. The results shown on Figs. 13 and 14 indicate that at constant nucleation site density, the heat transfer coefficient is a very weak function of the temperature difference. The results of the model agree with experimental results for temperature differences greater than one degree Fahrenheit. For small temperature differences, the data indicates a sharp decrease in the heat transfer coefficient and therefore, a sharp decrease in the active nucleation site density.

The radius of the minimum sized drop increases rapidly as the temperature difference is reduced below one degree Fahrenheit (Fig. 15). When the temperature difference decreases from one degree to one-quarter of a degree, the minimum drop radius increases by a factor of five! A typical surface is composed of sites which produce primary drops of different diameters. Normally there are many sites which produce small drops and a few sites which produce large primary drops. As the temperature difference decreases and the minimum drop radius increases, the small sites become inactive and the active site density decreases.

The dependence of the heat transfer coefficient on the total temperature cannot be explained by overlapping of large primary drops. At one-quarter degree temperature difference and an active site density of 10^8 sites/cm^2, less than ten per cent of randomly spaced primary drops overlap.

To facilitate measurement of the population of small drops, some investigations have used low temperature differences. If the temperature difference is small enough, it may be possible to

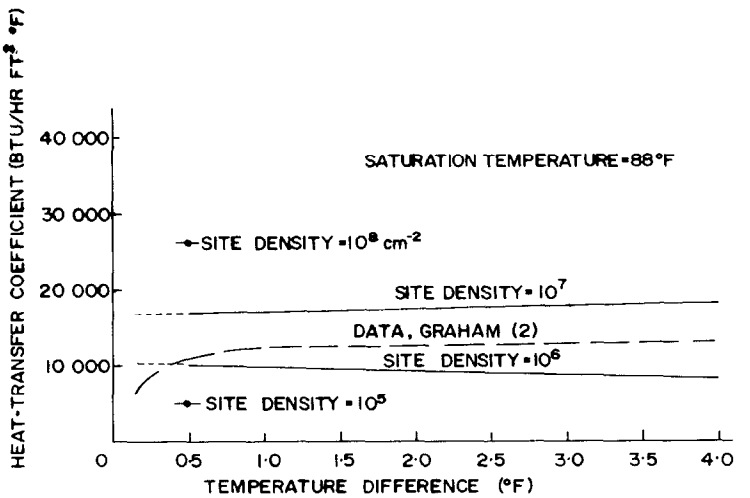

FIG. 13. Time-averaged heat transfer coefficient versus total temperature difference at a saturation temperature of 88°F.

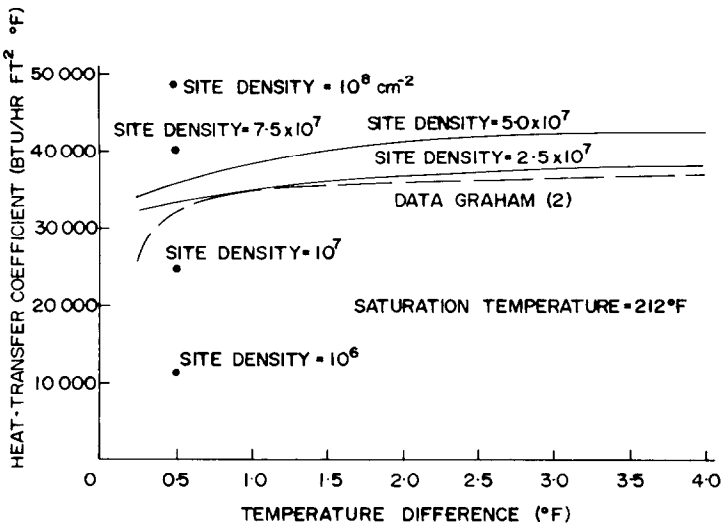

FIG. 14. Time-averaged heat transfer coefficient versus total temperature difference at a saturation temperature of 212°F.

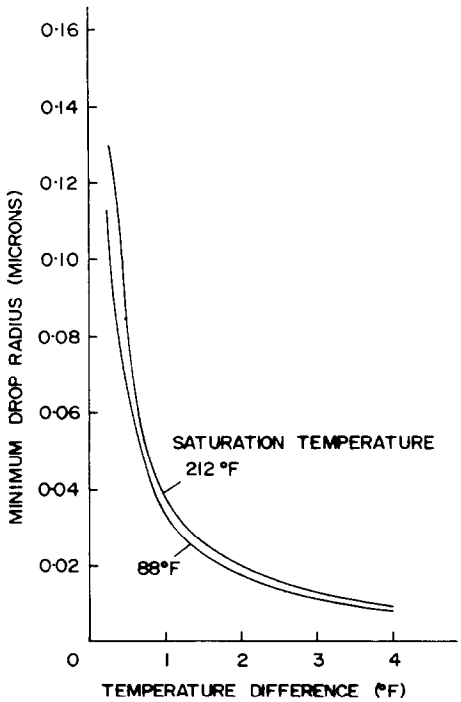

FIG. 15. Minimum radius of drop which can exist on condensing surface.

view all nucleating drops through a microscope However, the site density derived from these measurements will be much less than the active site density for typical operating conditions.

H. *Departing drop size*

As the size of departing drops increases, the cycle time increases and the average heat transfer coefficient decreases. For a given set of conditions, i.e. nucleation site density, total temperature difference, and pressure, the average heat transfer coefficient varies inversely with the cycle time to the one-quarter power. When the cycle time doubles, the heat transfer coefficient decreases by only twenty percent.

A simple relationship between the cycle time and the average heat transfer coefficient can be obtained when the departing drop size is constant. Since the large drops, which contain almost all the liquid on the surface, follow a universal size distribution, the amount of liquid condensed in one cycle is a constant when the size of the departing drop is a constant. The amount of liquid on the surface at the end of a cycle is given by

$$(\bar{h})(t)(\Delta T) = \text{Amount of liquid at time } t = \text{constant} \tag{11}$$

therefore:

$$t = \frac{\text{constant}}{\bar{h}\Delta T}. \tag{12}$$

Tower and Westwater [9] measured the average heat transfer coefficient and the cycle time for a plate inclined at various angles. The experiments were conducted with total temperature differences in the approximate range of 2–3°F. The departing drop diameter varied from 1900 to 2500 μ with cycle times from less than 1–1½ s, respectively. The experimental results of Tower and Westwater are shown on Fig. 16 for surfaces inclined both upward and downward. Theoretical results are shown for temperature differences of two and three degrees Fahrenheit, for four different site densities, and for two different cycle termination criteria: termination when the maximum drop diameter exceeds 1600 μ and 2500 μ, respectively. The agreement of the measured and predicted heat transfer coefficients is not a conclusive check of the theory since the site density is an independent variable in the calculations. The simultaneous agreement of the cycle times and heat transfer coefficients, however, is a conclusive check.

The calculated heat transfer coefficient decreases as the departing drop size is increased, as shown on Fig. 17. For a given site density and temperature difference, the relationship between the average heat transfer coefficient and the departing drop diameter is:

$$\frac{[\bar{h}(D_{\max})]}{[\bar{h}(D_{\max})_0]} = \left(\frac{D_{\max}}{(D_{\max})_0}\right)^{-\frac{1}{3}}. \tag{13}$$

The one-third power exponent holds for atmospheric pressure. At subatmospheric pressure the departing drop size has a weaker influence on the average heat transfer coefficient.

The results of this study can be used to explain the effect of surface inclination. However, it must be borne in mind that the model assumes all drops are hemispherical in shape. The size and shape of departing drops is found to change with inclination. Using the Macdougall–Ockrent expression [25] for the area of a departing drop projected in a vertical plane:

$$A = \frac{\sigma[\cos\theta_R - \cos\theta_A]}{\rho g \sin\alpha} \tag{14}$$

where α is the plate inclination from the hori-

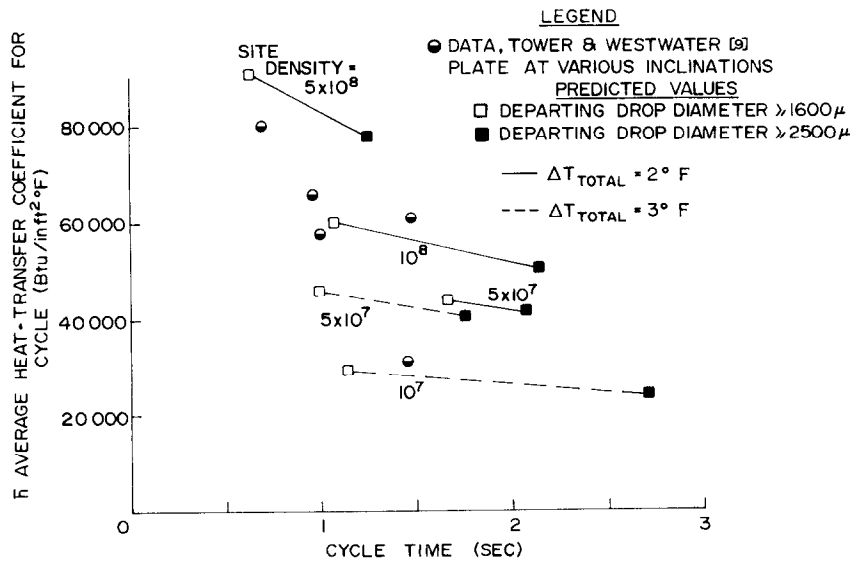

FIG. 16. A comparison of data and predictions for the average heat transfer coefficient and cycle time.

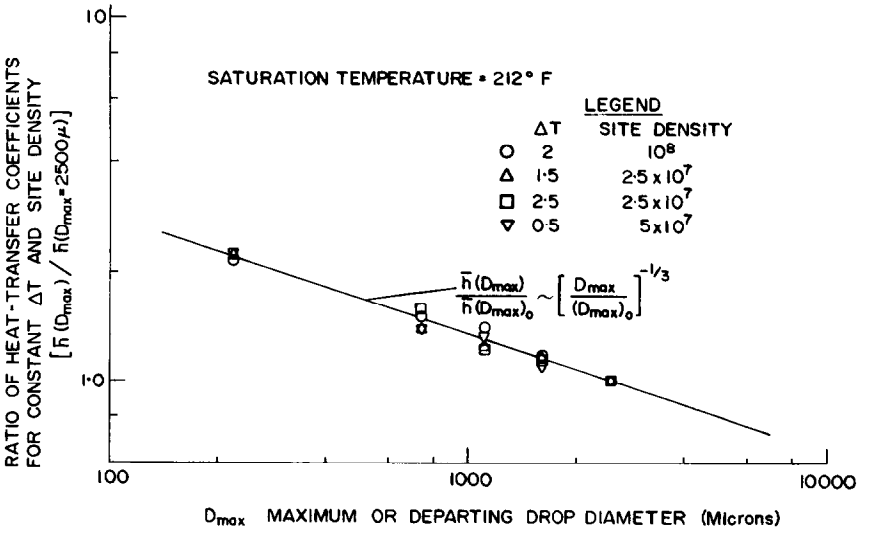

FIG. 17. Variation of time-averaged heat transfer coefficient with departing drop diameter.

zontal plane. For hemispherical drops:

$$A = \frac{\pi D_{\max}^2}{8}.$$

Therefore

$$D_{\max} \sim \left(\frac{\cos\theta_R - \cos\theta_A}{\sin\alpha}\right)^{\frac{1}{2}}. \qquad (15)$$

For atmospheric pressure, combining equations (13) and (15),

$$\bar{h} \sim \left(\frac{\sin\alpha}{\cos\theta_R - \cos\theta_A}\right)^{\frac{1}{4}}. \qquad (16)$$

For the limited range of inclination angles examined by Macdougall and Ockrent, the numerator of equation (15) was found to increase with inclination angle. On Fig. 18, the results of equation (16) are compared to the experimental data of Citakoglu and Rose [8] for two cases, assuming that the value of $|\cos\theta_R - \cos\theta_A|$ is a constant, and assuming the value is inversely proportional to sin α.

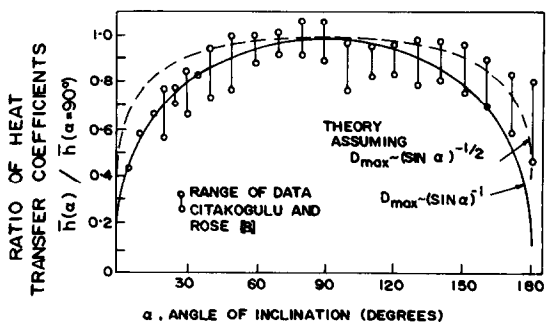

FIG. 18. Variation of time-averaged heat transfer coefficient with plate inclination ($\alpha = 0$ corresponds to horizontal plate facing upwards).

J. *Limitations of the model*

The cycle times are not predicted exactly with the current program. The time step sizes of final stage is two-tenths of a second or greater. When a drop of the maximum size is formed during a step, the cycle time at the end of the step is used. All drops are assumed to be hemispherical; if large drops are not hemispherical the growth time of the drop will be inaccurately predicted.

The simulation does not include the effect of sweeping. Actually, drops of the departing size slide down the surface and sweep vertical strips of the surface bare. Adjacent strips contain drops which are in different periods of the growth cycle. The drops in adjacent strips may interact to hasten the production of departing drops.

The size of the primary nucleating drops was taken to be a constant for a given saturation temperature and vapor-to-condensing surface

temperature difference. If the sizes of the primary drops were represented by a simple distribution function, e.g. a negative exponential, the fall-off of heat flux with temperature difference could be simulated. In addition, the experimental data at low temperature differences would provide information about the size distribution of nucleation sites.

6. CONCLUSIONS

In dropwise condensation, a majority of the condensation takes place on small drops for which conduction, interfacial, and curvature effects are all significant. Large drops grow by coalescence with small drops and the distribution of large drops follows a universal distribution.

The density of active nucleation sites is an important variable in determining the average heat transfer coefficient. McCormick and Westwater [11] reached the same conclusion from an examination of their experimental data. To determine the density of active nucleation sites, drops with diameters less than one micron must be counted. Counting only large drops results in large errors in the inferred nucleation site density when the heat transfer coefficient is greater than 10^4 Btu/(hft^2°F).

The average heat transfer coefficient varies weakly with size of the departing drops. This explains the minimal changes in heat transfer found for changes in plate inclination.

The observed decrease of the heat transfer coefficient at small temperature differences is not due to the kinematics of drop growth. Small nucleation sites become inactive at small temperature differences, reducing the active site density, and causing a decreased heat transfer coefficient.

The observed increase of the heat transfer coefficient with increased pressures at subatmospheric pressure levels is due to a decreased interfacial mass transfer resistance and to an increased density of active nucleation sites.

The agreement of the theoretical results with existing data indicates that the staging technique of modeling condensation gives valid results. The agreement also reaffirms the nucleation theory of condensation upon which the present calculations are based.

ACKNOWLEDGEMENTS

This work was supported in part by the Naval Ship Systems Command, Washington, D.C., and by a grant from the Shell Companies Foundation, Inc.

REFERENCES

1. E. Schmidt, W. Schurig and W. Sellschop, Versuche über die Kondensation von Wasserdampf un Film-und Tropfenform, *Tech. Mech. Thermo-Dynam., Berl.* **1**, 53 (1930).
2. C. Graham, The limiting heat transfer mechanisms of dropwise condensation, Ph.D. Thesis, Mass. Inst. Tech. (1969).
3. D. W. Tanner, D. Pope, C. J. Potter and D. West, Heat transfer in dropwise condensation at low steam pressures in the absence and presence of non-condensible gases, *Int. J. Heat Mass Transfer* **11**, 181 (1968).
4. H. Wenzel, Versuche über Tropfenkondensation, *Allg. Wärmetech.* **8**, 53 (1957).
5. D. W. Tanner, C. J. Potter, D. Pope and D. West, Heat transfer in dropwise condensation—Part I, *Int. J. Heat Mass Transfer* **8**, 419 (1965).
6. E. J. LeFevre and J. W. Rose, An experimental study of heat transfer by dropwise condensation, *Int. J. Heat Mass Transfer* **8**, 1117 (1965).
7. C. Citakoglu and J. W. Rose, Dropwise condensation —some factors influencing the validity of heat transfer measurements, *Int. J. Heat Mass Transfer* **11**, 523 (1968).
8. E. Citakoglu and J. W. Rose, Dropwise condensation —The effect of surface inclination, *Int. J. Heat Mass Transfer* **12**, 645 (1969).
9. R. E. Tower and J. W. Westwater, Effect of plate inclination on heat transfer during dropwise condensation of steam, *Chem. Engng Prog. Symp. Ser.* **66** (102), 21–25 (1970).
10. A. Umur and P. Griffith, Mechanism of dropwise condensation, *J. Heat Transfer* **87**, 275 (1966).
11. J. L. McCormick and J. W. Westwater, Drop dynamics and heat transfer during dropwise condensation of water vapor on a horizontal surface, *Chem. Engng Prog. Symp. Ser.* **62** (64), 120 (1966).
12. J. L. McCormick and J. W. Westwater, Nucleation sites for dropwise condensation, *Chem. Engng Sci.* **20**, 1021 (1965).
13. A. C. Peterson and J. W. Westwater, Dropwise condensation of ethylene glycol, *Chem. Engng Prog. Symp. Ser.* **62** (64), 135 (1966).
14. N. Fatica and D. L. Katz, Dropwise condensation, *Chem. Engng. Prog.* **45**, 661 (1949).
15. S. Sugawara and I. Michiyoshi, Dropwise condensation, *Mem. Fac. Engng Kyoto Univ.* **18** (2), 84 (1956).

16. H. WENZEL, Der Wärmeübergang bei der Tropfenkondensation, *Linde-Ber. Tech. Wiss.* **18**, 44 (1964).
17. E. J. LE FEVRE and J. W. ROSE, A theory of heat transfer by dropwise condensation, *Proc. Third Int. Heat Transfer Conference*, Am. Inst. Chem. Engrs. New York, No. 2, p. 362 (1966).
18. L. R. GLICKSMAN and J. W. ROSE, Dropwise condensation—the distribution of drop sizes, submitted to *Int. J. Heat Mass Transfer*.
19. E. E. GOSE, A. N. MUCCIARDI and E. BAER, Model for dropwise condensation on randomly distributed sites, *Int. J. Heat Mass Transfer* **10**, 15 (1967).
20. I. TANASAWA and F. TACHIBANA, A synthesis of the total process of dropwise condensation using the method of computer simulation, *Proc. Fourth Int. Heat Transfer Conference*, 6, Paper Cs 1.3 (1970).
21. B. MIKIC, On the mechanism of dropwise condensation, *Int. J. Heat Mass Transfer* **12**, 1311 (1969).
22. R. W. SCHRAGE, *A Theoretical Study of Interphase Mass Transfer*. Columbia University Press, New York (1953).
23. W. ROHSENOW and S. WILCOX, Film condensation of potassium using copper condensing block for precise wall temperature measurement, *J. Heat Transfer* **92C**, 359–371 (1970).
24. S. KRISCHER and U. GRIGULL, Microscopic study of dropwise condensation, *Wärme und Stoffbertragung* **4**, 48–59 (1971).
25. G. MACDOUGALL and C. OCKRENT, Surface energy relations in liquid/solid systems, *Proc. R. Soc., Lond.* **180A**, 151–173 (1942).

SIMULATION NUMERIQUE DE LA CONDENSATION EN GOUTTE

Résumé—On réalise une simulation numérique du transfert thermique lors de la condensation en goutte, La simulation porte sur la croissance, la coalescence et la renucléation de gouttes appartenant à un domaine de taille depuis les plus petites gouttes nucléées jusqu'aux gouttes qui se détachent. Les calculs sont menés avec une densité de sites actifs atteignant 10^9 sites/cm^2.

Le transfert thermique à la goutte a été déterminé en considérant les effets de courbure de la surface de la goutte, le transfert massique interfacial entre les phases liquide et vapeur, la conduction à travers la goutte. On omet les effets des incondensables dans la vapeur et de la conduction non uniforme dans le matériau sur la surface duquel se fait la condensation.

Le coefficient de transfert thermique est fonction de la densité en sites actifs, de la température de saturation, de la taille de la goutte qui se détache et de la différence de température entre la vapeur et la surface. Les résultats sont en bon accord avec les résultats expérimentaux disponibles.

NUMERISCHE BERECHNUNG DER TROPFENKONDENSATION

Zusammenfassung– Eine numerische Berechnung des Wärmeüberganges bei Tropfenkondensation wurde durchgeführt. Die Berechnung efasst das Wachstum, die Verschmelzung und Reaktivierung von Keimen in der Grösse kleinster bis zu abfallenden Tropfen.

Die Berechnungen wurden mit einer Keimdichte von 10^9 Keimen pro cm^2 durchgeführt. Der Wärmeübergang am Tropfen wurde durch Betrachtungen der Oberflächenspannung des Tropfens. des Massentransportes an der Phasengrenze zwischen flüssiger und dampfförmiger Phase und durch Betrachtung der Leitfähigkeit des Tropfens bestimmt.

Die Effekte von Inertanteilen in Dampf und ungleichmässiger Wärmeleitung in der Kühlfläche blieben unberücksichtigt. Der Wärmeübergangskoeffizient wurde als Funktion der aktiven Keimdichte. der Sättigungstemperatur, der Grösse der abfallenden Tropfen und der Temperaturdifferenz zwischen Dampf- und Kühlflächen gefunden. Die Ergebnisse stimmen gut mit den verfügbaren experimentellen Ergebnissen überein.

ЧИСЛЕННОЕ МОДЕЛИРОВАНИЕ ПРОЦЕССА КАПЕЛЬНОЙ КОНДЕНСАЦИИ

Аннотация—Выполнено численное моделирование процесса теплообмена при капельной конденсации. При этом учитывались рост, слияние и дробление капель различного размера — от самых мелких (ядер конденасции) до отрывающихся капель. Расчет проводился для плотности центров конденсации порядка 10^9 на см^2.

Теплообмен капли определялся с учетом кривизны ее поверхности, массообмена между жидкой и паровой фазами и теплопроводности капли. Влияние неконденсирующихся компонентов и неоднородной теплопроводности не учитывалось. Коэффициент теплообмена находился в зависимости от плотности активных центров, температуры насыщения, размера отрывающихся капель и перепада температур между паром и поверхностью. Результаты хорошо согласуются с известными экспериментальными данными.